Dynamics of Atmospheres and Oceans, 14 (1990) 229–258
Elsevier Science Publishers B.V., Amsterdam – Printed in The Netherlands

THE MODELLING OF THE FLOW OF WATER THROUGH THE BOSPHORUS

B. JOHNS

Department of Meteorology, University of Reading, Reading (England)

T. OGUZ

Institute of Marine Sciences, Middle East Technical University, Erdemli, Icel (Turkey)

(Received October 5, 1988; revised March 20, 1989; accepted May 25, 1989)

ABSTRACT

Johns, B. and Oguz, T., 1990. The modelling of the flow of water through the Bosphorus. Dyn. Atmos. Oceans, 14:229–258

A numerical model is developed for the exchange of water between the Black Sea and the Marmara Sea through the Bosphorus. An essential part of the modelling procedure is the use of a turbulence energy equation in a scheme of turbulence parameterization. The simultaneous application of a transport equation for the salinity leads to a turbulence suppression term associated with the existence of a strongly stable vertical salinity stratification. Experiments are performed that show how a prescribed difference between the salinities of the Black Sea and the Marmara Sea leads to a basically two-layer flow structure in the model strait. The detailed structure of the flow is complex and involves an intermediate entrainment layer in which there is a system of recirculation that may be expected to play a prominent role in the exchange of water properties between the surface and bottom layers. It is tentatively suggested that the presence of a model sill adjacent to the Marmara Sea may lead to an interpretation of the local flow regime in terms of a stationary internal hydraulic jump phenomenon.

1. INTRODUCTION

The marine waterway linking the Aegean Sea to the Black Sea is a classic example of a two-layer flow system. A source of relatively fresh water originating in the Black Sea (and resulting from river run-off) supports the driving mechanism for the near-surface flow. Thus, there is a continuing outflow of water from the Black Sea through the Bosphorus and into the Marmara Sea. This flow persists throughout the Turkish Straits and eventually exits from the Dardanelles into the Aegean Sea. The flow in the lower

0377-0265/90/$03.50

layer, however, is in the opposite direction to that in the upper layer and is a consequence of the marked difference between the ambient salinities of the Aegean Sea and the Black Sea. Lower-layer water of Aegean origin flows through the Turkish Straits and eventually exits from the Bosphorus into the Black Sea. Naturally, the detailed form of this general flow pattern depends on seasonal variations in the outflow of fresh water and variations in the applied sea-surface wind-stress forcing

In the present work, we are concerned solely with an evaluation of the dynamical processes in the Bosphorus itself and do not consider the circulation in the adjacent seas. The general structure of the flow regime in the Bosphorus is well understood and was first systematically investigated by Merz and Möller whose principal results were documented by Defant (1961). An excellent review of the latest observational work (including important contributions by Ünlüata and Oguz (1983)) was given by Tolmazin (1985). These studies showed that each flow regime has a distinct wedge-like structure and accommodates stronger currents at its point of communication with the sea of destination. Moreover, there is relatively little mixing across the interface separating the two layers, as is evidenced by the abrupt change in the salinity which can amount to 18 ppt over a depth of 10 m. Consequently, the two layers retain their essential identity over the 32 km separating the Marmara Sea from the Black Sea. For this reason, theoretical investigations into the exchange of water through the Bosphorus have been based on the application of steady-state dynamical models in which there are two immiscible layers of fluid of prescribed density.

The application of a simple two-layer model to the Bosphorus was described by Defant (1961). In this, a hydrostatically derived pressure gradient is balanced by an internal frictional force. Thus, the model includes contributions to the pressure gradient derived from both the slope of the free surface and that of the interface separating the two layers. With an appropriate choice of frictional, density and geometrical parameters, the model yields expressions for the interfacial slope, and the current profiles in each layer, in terms of the slope of the free surface. The general picture that emerges is in accord with observation and implies oppositely directed currents in each layer.

More sophisticated theoretical analyses have been given for two-layer systems by Assaf and Hecht (1974) and Sumer and Bakioglu (1981) and their principal conclusions were reviewed by Tolmazin (1985). A two-dimensional model for the stratified flow in a strait of constant breadth and variable depth was described by Tolmazin (1981). In this, a longitudinal gravitational circulation is maintained by the imposition of density and elevation differences between adjacent seas. Numerical evaluations show there to be a broad measure of agreement between the model results and the

gross observed characteristics of the flow through Bosphorus. An informative and related contribution was given by Wang (1987) who uses a three-dimensional numerical primitive equation model to study the circulation in a strait with special emphasis being given to the effect of buoyancy on strait outflow.

One of the most striking features of the water exchange through the Bosphorus is the apparently intense vertical mixing found on the Marmara Sea side of a sill situated in mid-stream off Istanbul. Clear evidence of this is obtained from infra-red satellite photographs which show a zone of relatively cold surface water near to the point of entry of the Bosphorus into the Marmara Sea. This cold water is presumably of bottom origin and has been brought to the surface by the action of dynamical processes uniquely related to the presence of the sill.

The cause of this surfacing of bottom water (also confirmed by an observed increase in the surface salinity) has been attributed to the formation of a stationary internal hydraulic jump in the vicinity of the sill. This would lead to an enhanced local production of turbulence which would then intensify the vertical mixing of water properties.

In the present paper we have developed a multi-level two-dimensional channel model of the flow through the Bosphorus. A scheme of turbulence parameterization is applied which is based on that used in previous modelling studies by Johns (1978, 1983). In these, turbulence closure was achieved at the level of the turbulence energy equation. In the work presented here, we have added a transport equation to the system which describes how salinity is advected and diffused through the channel. The inclusion of this process leads to an extra term in the turbulence energy equation. This has its maximal effect in regions of strongly stable vertical salinity stratification where it has a marked suppressive influence on turbulence generation. Thus, we have included a process that is compatible with the development of an effectively two-layer flow system in which there is only a weak vertical mixing of water properties between the two layers.

The form of the boundary conditions to be applied on the salinity at the ends of the channel is central to our modelling procedure. These conditions state that during inflow from an adjacent sea into the channel the salinity is prescribed. During outflow from the channel into an adjacent sea, however, the salinity is determined from the model equations. The flow in the channel is maintained by the application of a boundary condition at its Black Sea end and this leads to a volume flux of water into the channel.

The boundary conditions to be imposed at the ends of the model channel are formulated so as to apply to assumed subcritical flow conditions. Thus, we have arranged that the end regions of the channel do not include either the abrupt expansion, corresponding to where the Bosphorus joins the

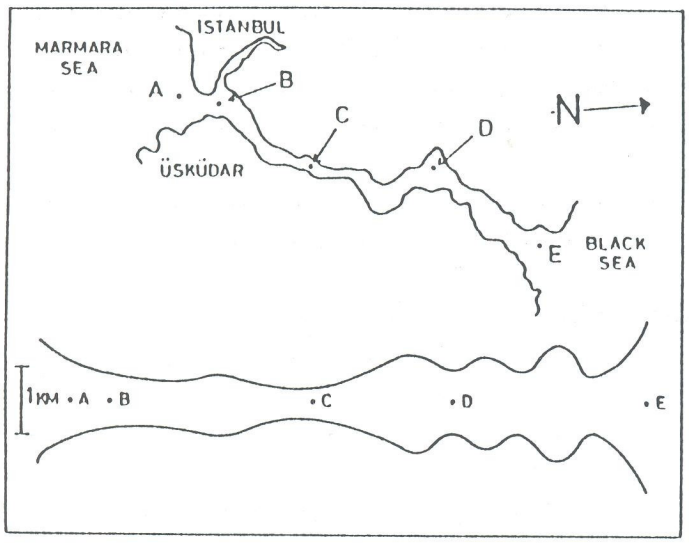

Fig. 1. Topography of the Bosphorus Strait and a diagrammatic plan of its one-dimensional channel representation.

Marmara Sea, or the sill near where the Bosphorus communicates with the Black Sea. Accordingly, there is no necessity to invoke the concept of hydraulic control at the ends of the model channel. Any supercritical flow conditions existing within the channel will appear as a consequence of the solution of the governing equations of the model.

Using this model, we have performed numerical experiments on the flow through the Bosphorus for which there is a realistic incorporation of topography and bathymetry. In particular, we have included a representation of the sill adjacent to the Marmara Sea. Evaluations are made of salinity and current distribution along the channel and, wherever possible, these are compared with observational data. We also determine the streamlines of the flow through the channel and, on the basis of these, have identified the position of the sill with a region in which there may be a formation of a stationary internal hydraulic jump.

2. FORMULATION OF MODEL EQUATIONS

The Bosphorus is modelled by a channel having a variable, but prescribed, rectangular cross-section. A diagrammatic sketch of this arrangement is shown in Fig. 1. The origin, O, of the longitudinal axis Ox is located at the southwestern extremity of the channel corresponding to its point of communication with the Marmara Sea. The northeastern extremity corresponds to the point at which the Bosphorus enters the Black Sea and this is given by $x = L$. The origin, O, is located within the undisturbed free surface

of the water in the channel and an axis, Oz, is directed vertically upwards from $z = 0$. At position x and at time t, the location of the disturbed free surface is given by $z = \zeta(x, t)$. The impermeable floor of the channel corresponds to $z = -h(x)$ and its breadth is denoted by $b(x)$.

We denote the Reynolds-averaged components of the fluid velocity by (u, w) and invoke a hydrostatic pressure approximation and a Boussinesq approximation. The momentum equation then has the form

$$\frac{\partial}{\partial t}(bu) + \frac{\partial}{\partial x}(bu^2) + \frac{\partial}{\partial z}(buw) = -gb\frac{\partial \zeta}{\partial x} - \frac{b}{\rho_0}\int_z^\zeta \frac{\partial}{\partial x}(g\rho)\,\mathrm{d}z + \frac{\partial}{\partial z}\left[K_M \frac{\partial}{\partial z}(bu)\right] + \mathscr{L}(u) \tag{2.1}$$

The first term on the right-hand-side of eqn. (2.1) gives the barotropic contribution to the pressure gradient resulting from the slope of the free surface in the channel. In the Bosphorus, the existence of such a slope is a consequence of the source of fresh water originating in the Black Sea. This derives from river discharge and an excess of precipitation over evaporation thus leading to $(\partial\zeta/\partial x) > 0$. It therefore implies a surface flow towards the Marmara Sea. The second term, in which ρ_0 is the density of fresh water, gives the baroclinic contribution to the pressure gradient. This results from a horizontal gradient in the density, ρ, consequent upon the different ambient salinities of the water in the Black Sea and Marmara Sea. The third term represents a vertical transfer of momentum by turbulent motions and is expressed in terms of a conventional gradient law involving a vertical coefficient of eddy viscosity, K_M. In the final term, $\mathscr{L}$ is an operator such that $\mathscr{L}(u)$ simulates the effect of horizontal momentum exchange by turbulent scale motions. The inclusion of such a term is required because of the anticipated formation of an internal hydraulic jump in the Bosphorus.

The equation of continuity in the channel is

$$\frac{\partial}{\partial x}(bu) + \frac{\partial}{\partial z}(bw) = 0 \tag{2.2}$$

Equivalently, this may be written in the form

$$b\frac{\partial H}{\partial t} + \frac{\partial}{\partial x}(bH\bar{u}) = 0 \tag{2.3}$$

where H is the total depth, $\zeta + h$, and $\bar{u}$ is the depth-averaged velocity given by

$$\bar{u} = \frac{1}{H}\int_{-h}^{\zeta} u\,\mathrm{d}z \tag{2.4}$$

The density, ρ, is related to the salinity, S, by an equation of state in which

$$\rho = \rho_0(1 + \gamma S) \tag{2.5}$$

where we take $\gamma = 7.5 \times 10^{-4}$/ppt.

The salinity is determined from a transport equation having the form

$$\frac{\partial}{\partial t}(bS) + \frac{\partial}{\partial x}(buS) + \frac{\partial}{\partial z}(bwS) = \frac{\partial}{\partial z}\left[K_S \frac{\partial}{\partial z}(bS)\right] + \mathscr{L}(S) \tag{2.6}$$

On the right-hand-side of eqn. (2.6), the vertical transfer of salinity by turbulent processes is represented in terms of a gradient transfer law with an eddy coefficient, K_S. The final term represents the effect of a turbulent horizontal salinity flux which, in comparison with the horizontal advective salinity flux, is expected to be of secondary importance.

The parameterization of the turbulent processes is completed by the introduction of a transport equation for the turbulence energy density, E. This has the form

$$\frac{\partial}{\partial t}(bE) + \frac{\partial}{\partial x}(buE) + \frac{\partial}{\partial z}(bwE) = bK_M\left(\frac{\partial u}{\partial z}\right)^2 + P + \frac{g}{\rho_0} bK_S \frac{\partial \rho}{\partial z} + \frac{\partial}{\partial z}\left[K_E \frac{\partial}{\partial z}(bE)\right] + \mathscr{L}(E) - b\epsilon \tag{2.7}$$

On the right-hand-side of eqn. (2.7), the first term represents a production of turbulence energy consequent upon there being a vertical shear in the Reynolds-averaged flow. The second term represents a production of turbulence energy associated with the action of the normal eddy stresses. These terms describe the ways in which energy may be transferred from the Reynolds-averaged flow to the turbulence energy budget. For $(\partial\rho/\partial z) < 0$, the third term represents a sink of turbulence energy resulting from the presence of a stable density stratification. The fourth term represents a vertical diffusion of turbulence energy with an eddy coefficient, K_E. The fifth term represents the horizontal redistribution of turbulence energy by the turbulence itself. The final term, involving ϵ, simulates the dissipation of turbulence energy.

In contrast with a scheme of parameterization based on a Richardson-number-dependent exchange coefficient, it should be noted that our scheme remains valid even when the stratification becomes locally unstable (Kundu, 1984). In these circumstances, the buoyancy term in eqn. (2.7) acts as a source of turbulence energy thus increasing the value of E and enhancing the vertical turbulent mixing. Moreover, our application of this scheme of parameterization appears to be particularly relevant in connection with the

enhancement of the horizontal turbulent mixing due to the development of any strong horizontal gradients in the flow field. The horizontal production term, P, (defined precisely in eqn. (3.10)) then enters importantly into the turbulence energy budget and its effect is to support the transfer of energy from the Reynolds-averaged flow into the turbulence energy budget. As will be seen later, this aspect of the parameterization is also of crucial relevance in the maintenance of a stable scheme of numerical solution but it contains an important physical content wherever there is a tendency for the formation of an internal hydraulic jump.

Finally, it must be emphasized that the parameterizations described here relate only to sub-grid-scale turbulent processes that cannot be resolved in our scheme of numerical solution. These are principally of importance in the bottom-boundary layer and become less so in the regions of strong vertical stratification that are anticipated to exist in regions separating the upper-layer flow from the lower-layer flow. There are, indeed, important exchange processes that take place between these layers but they are on a scale larger than that of turbulence. One of our principal results is the simulation of these larger-scale processes, the analysis of which leads to an understanding of the way in which salt, and other properties of the fluid, can be transferred between the upper and lower layers of the flow field.

Boundary conditions to accompany eqn. (2.7) state that there is no diffusive flux of turbulence energy across the floor of the channel and the free surface and these lead to

$$\frac{\partial E}{\partial z} = 0 \qquad \text{at } z = -h \qquad \text{and } z = \zeta \tag{2.8}$$

The various eddy coefficients appearing in the formulation are now expressed in terms of the turbulence energy density. In the present work, we take

$$K_M = K_S = K_E = K \tag{2.9}$$

and, following Johns (1978), write

$$K = c^{1/4} l E^{1/2} \tag{2.10}$$

Here, l is a vertical mixing length scale and c is an empirical constant. The vertical mixing length scale is given by

$$l = l_0 \exp\left[-\tfrac{1}{4}\beta(z+h)\right] \tag{2.11}$$

where l_0 is determined from the type of similarity hypothesis used by Johns (1978). Accordingly,

$$l_0 = -\frac{kE^{1/2}/l_0}{\dfrac{\mathrm{d}}{\mathrm{d}z}\left(E^{1/2}/l_0\right)}, \qquad l_0 = kz_0 \qquad \text{at } z = -h \tag{2.12}$$

where k is von Karman's constant (taken as 0.4) and z_0 is the roughness length of the elements at the floor of the channel.

In eqn. (2.10), β is an inverse length scale and, for $\beta(z+h) \ll 1$, $l \cong l_0$. The additional disposable parameter, β, is included because we have considerable evidence showing that the choice $\beta = 0$ (and therefore $l = l_0$) leads to an excessive mixing in the vertical and a failure of the model equations to predict the correct type of vertical structure in the velocity field.

The dissipation term in eqn. (2.7) is parameterized by writing

$$\epsilon = \frac{c^{3/4}E^{3/2}}{l_D} \tag{2.13}$$

where the dissipation length scale, l_D, is given by

$$l_D = l_0 \exp\left[\tfrac{3}{4}\beta(z+h)\right] \tag{2.14}$$

These equations must be accompanied by appropriate dynamical boundary conditions through which the system is driven.

At the floor of the channel, we apply a no-slip condition and take

$$u = 0 \qquad \text{at } z = -h \tag{2.15}$$

We prescribe zero applied surface wind stress and accordingly take

$$\frac{\partial u}{\partial z} = 0 \qquad \text{at } z = \zeta \tag{2.16}$$

Thus, the fluid motion in the channel is driven solely by boundary forcing to be applied at the extremities of the channel where it joins with the adjacent seas. This part of the specification is problematical because whatever conditions are applied must allow for the formation of oppositely directed surface and bottom flows. Because the near-surface flow through the Bosphorus is a consequence of an excess of fresh water originating in the Black Sea, it appears reasonable to prescribe a boundary condition at $x = L$ that, on the basis of a linearized frictionless analysis, is consistent with there being a barotropic transport through the strait. Invoking the type of condition used by Johns et al. (1983), which is based on the specification of conditions on an incoming characteristic, we have taken

$$\bar{u} - \left(\frac{g}{h}\right)^{1/2}\zeta = -2u_L \qquad \text{at } x = L \tag{2.17}$$

Here, u_L is a disposable parameter which, for a steady-state forcing, is a constant velocity. Thus, eqn. (2.17) relates the surface elevation and the depth-averaged current at the northeastern extremity of the Bosphorus. At the Marmara Sea end, we apply a similar condition which, ideally, would

allow for the free outward transmission from the analysis region of the entire barotropic response reaching $x = 0$. This has the form

$$\bar{u} + \left(\frac{g}{h}\right)^{1/2} \zeta = 0 \qquad \text{at } x = 0 \tag{2.18}$$

It will be noted that eqns. (2.17) and (2.18) do not involve the prescription of a velocity profile at the ends of the channel. They are not, therefore, incompatible with the development of a two-layer velocity structure determined by the salinity contrast existing between the Black Sea and the Marmara Sea.

To allow for the formation of a horizontal salinity structure within the channel, it is necessary that the boundary conditions to accompany eqn. (2.6) be correctly formulated. Essentially, the conditions to be applied at $x = 0$ and $x = L$ must be such that the salinity of inflowing water is prescribed and that of the outflowing water is determined by use of eqn. (2.6). Therefore, during inflow at $x = 0$ (when $u > 0$), we take

$$S = S_0 \tag{2.19}$$

During inflow at $x = L$ (when $u < 0$), we take

$$S = S_L \tag{2.20}$$

S_0 and S_L are constant salinities based on observations made in the adjacent seas.

Further conditions to accompany eqn. (2.6) require that there be no diffusive flux of salinity across the floor of the channel and the free surface, and these lead to

$$\frac{\partial S}{\partial z} = 0 \qquad \text{at } z = -h \qquad \text{and } z = \zeta \tag{2.21}$$

A final comment is appropriate concerning the representation of K in terms of E. Assuming, near $z = -h$, that eqn. (2.7) reduces to a balance between the production and dissipation terms, we obtain

$$K\left(\frac{\partial u}{\partial z}\right)^2 = \epsilon \tag{2.22}$$

because $u = 0$ and $\partial\rho/\partial z = 0$ at $z = -h$.
Accordingly

$$l l_D \left(\frac{\partial u}{\partial z}\right)^2 \sim e^{1/2} E \qquad \text{as } z \to -h \tag{2.23}$$

leading to

$$K = \left(l^3 l_D\right)^{1/2} \left|\frac{\partial u}{\partial z}\right| \sim (k z_0)^2 \left|\frac{\partial u}{\partial z}\right| \qquad \text{as } z \to -h \tag{2.24}$$

which is consistent with Prandtl's mixing length theory for conditions of neutral stability.

In accordance with previous work (Johns, 1978), we take $c = 0.08$.

3. COORDINATE TRANSFORMATION

Following Johns (1978), it is convenient to make a coordinate transformation that facilitates the fulfilment of the boundary conditions at $z = -h$ and $z = \zeta$. This has the form

$$\sigma = \frac{z + h}{H} \tag{3.1}$$

so that the floor of the channel and the free surface correspond respectively to $\sigma = 0$ and $\sigma = 1$. New prognostic variables are defined by

$$\left.\begin{aligned} \tilde{u} &= bHu \\ \tilde{S} &= bHS \\ \tilde{E} &= bHE \end{aligned}\right\} \tag{3.2}$$

Using x, σ and t as new independent variables and substituting for ρ from eqn. (2.5), we find that eqn. (2.1) leads to

$$\begin{aligned} &\frac{\partial \tilde{u}}{\partial t} + \frac{\partial}{\partial x}(u\tilde{u}) + \frac{\partial}{\partial \sigma}(\omega \tilde{u}) \\ &\quad = -gbH\frac{\partial \zeta}{\partial x} - g\gamma bH^2 \int_\sigma^1 \frac{\partial S}{\partial x}\, d\sigma + g\gamma bH\left[\left\{(1-\sigma)S - \int_\sigma^1 S\, d\sigma\right\}\frac{\partial h}{\partial x}\right. \\ &\qquad \left. + \left\{S_{\sigma=1} - \sigma S - \int_\sigma^1 S\, d\sigma\right\}\frac{\partial \zeta}{\partial x}\right] + \frac{1}{H^2}\frac{\partial}{\partial \sigma}\left(K\frac{\partial \tilde{u}}{\partial \sigma}\right) + H\mathscr{L}(u) \end{aligned} \tag{3.3}$$

In eqn. (3.3), the new dependent variable, ω, is defined by

$$\omega = \sigma_t + u\sigma_x + w\sigma_z \tag{3.4}$$

where a subscript denotes a partial differentiation.

A complete development of $\mathscr{L}(u)$ using a formal parameterization involving a horizontal eddy coefficient, N, leads to

$$\mathscr{L}(u) = \left(\frac{\partial}{\partial x} + \sigma_x\frac{\partial}{\partial \sigma}\right)\left[bN\left(\frac{\partial u}{\partial x} + \sigma_x\frac{\partial u}{\partial \sigma}\right)\right] \tag{3.5}$$

However, because our principal requirement is that we apply a mixing process that smoothes out any developing discontinuity associated with the formation of an internal hydraulic jump, we have chosen to replace eqn. (3.5) by

$$\mathscr{L}(u) = \frac{1}{H}\frac{\partial}{\partial x}\left(bHN\frac{\partial u}{\partial x}\right) \tag{3.6}$$

In view of the crude parameterizations involved, and the uncertain value to be assigned to N, there appears to be little merit in retaining the full form of $\mathscr{L}(u)$ given in eqn. (3.5).

Transformation of eqn. (2.2) leads to a purely diagnostic equation for ω in which

$$\frac{\partial}{\partial x}\{bH(u-\bar{u})\}+\frac{\partial}{\partial \sigma}(bH\omega)=0 \tag{3.7}$$

where $\omega=0$ at $\sigma=0$ and $\sigma=1$.

Equation (2.6) leads to

$$\frac{\partial \tilde{S}}{\partial t}+\frac{\partial}{\partial x}(u\tilde{S})+\frac{\partial}{\partial \sigma}(\omega\tilde{S})=\frac{1}{H^2}\frac{\partial}{\partial \sigma}\left(K\frac{\partial \tilde{S}}{\partial \sigma}\right)+\frac{\partial}{\partial x}\left(bHN\frac{\partial S}{\partial x}\right) \tag{3.8}$$

where we have used an approximation for $\mathscr{L}(s)$ similar to that used in (3.6). Likewise, eqn. (2.7) becomes

$$\frac{\partial \tilde{E}}{\partial t}+\frac{\partial}{\partial x}(u\tilde{E})+\frac{\partial}{\partial \sigma}(\omega\tilde{E})=\frac{bK}{H^3}\left(\frac{\partial \tilde{u}}{\partial \sigma}\right)^2+HP+gb\gamma K\frac{\partial S}{\partial \sigma}+\frac{1}{H^2}\frac{\partial}{\partial \sigma}\left(K\frac{\partial \tilde{E}}{\partial \sigma}\right)+\frac{\partial}{\partial x}\left(bHN\frac{\partial E}{\partial x}\right)-bH\epsilon \tag{3.9}$$

A necessary requirement is that eqns. (3.3) and (3.9) be energetically consistent. This means that the implied loss of energy from the Reynolds-averaged flow must be balanced by a corresponding increase in the turbulence energy density. In eqn. (3.9), this is achieved by taking

$$P=bN\left(\frac{\partial u}{\partial x}\right)^2 \tag{3.10}$$

The boundary conditions to accompany this set of transformed equations are now conveniently expressed at either $\sigma=0$ or $\sigma=1$.

Equations (2.15) and (2.16) lead to

$$u=0 \qquad \text{at } \sigma=0 \tag{3.11}$$

$$\frac{\partial u}{\partial \sigma}=0 \qquad \text{at } \sigma=1 \tag{3.12}$$

whereas eqns. (2.8) and (2.21) are equivalent to

$$\left.\begin{aligned}\frac{\partial E}{\partial \sigma}&=0\\ \frac{\partial S}{\partial \sigma}&=0\end{aligned}\right\} \qquad \text{at } \sigma=0 \quad \text{and } \sigma=1 \tag{3.13}$$

The forcing conditions (2.17) and (2.18) have an unchanged form but the depth-averaged velocity, $\bar{u}$, is now given by

$$\bar{u} = \int_0^1 u \, d\sigma \tag{3.14}$$

4. METHOD OF NUMERICAL SOLUTION

The equations described in section 3 will be solved on a finite-difference grid in the x–σ domain. We define

$$\left.\begin{aligned} x &= (i-1)\Delta x, \qquad i = 1, 2, \ldots, m, \qquad \Delta x = L/(m-1) \\ \sigma &= (j-1)\Delta\sigma, \qquad j = 1, 2, \ldots, n, \qquad \Delta\sigma = 1/(n-1) \end{aligned}\right\} \tag{4.1}$$

A discrete sequence of time-instants is defined by

$$t = p\Delta t, \qquad p = 0, 1, 2, \ldots. \tag{4.2}$$

The finite sequence of x-values consists of points of two distinct types. Odd values of i correspond to positions at which we evaluate the dependent variables ζ and $\tilde{S}$. Even values of i correspond to positions at which we evaluate the dependent variables $\tilde{u}$ and $\tilde{E}$. We choose m to be odd so that the end points of the computational domain correspond to ζ-points. The formal discretizations of eqns. (2.1), (2.3) and (3.3) follow those described by Johns (1978) and are not repeated here. It is, however, worthwhile to repeat the method of implementing eqns. (2.17) and (2.18) as this is crucial to the solution procedure.

We use a conventional subscript notation to reference grid-point values of the dependent variables and denote the time-level by a superscript. In practice, we apply eqn. (2.17) at $x = L - \Delta x$ which is a u-point. Furthermore, we evaluate the depth-averaged velocity at the lower time-level, thus introducing an error $O(\Delta t)$. This is consistent with the formal truncation error already present in our implicit evaluation of the vertical diffusion terms. Therefore, we write eqn. (2.17) as

$$\bar{u}^p_{m-1} - \frac{1}{2}\left(\frac{g}{h_{m-1}}\right)^{1/2}\left(\zeta^{p+1}_m + \zeta^{p+1}_{m-2}\right) = -2u_L \tag{4.3}$$

Because the elevation, ζ, is not carried at $i = m-1$ we have replaced its value there by the average of its values at the two adjacent ζ-points. Equation (4.3) then leads to

$$\zeta^{p+1}_m = -\zeta^{p+1}_{m-2} + 2\left(\frac{h_{m-1}}{g}\right)^{1/2}\left(2u_L + \bar{u}^p_{m-1}\right) \tag{4.4}$$

Thus, eqn. (4.4) yields a method of updating ζ at $x = L$ which utilizes an already-known interior updated value of ζ together with the depth-averaged velocity derived from the previous time-step.

In a similar manner, eqn. (2.18) leads to

$$\zeta_1^{p+1} = -\zeta_3^{p+1} - 2\left(\frac{h_2}{g}\right)^{1/2} \bar{u}_2^p \tag{4.5}$$

A description of the method of implementation of conditions having this form is given by Johns et al. (1981).

The solution of eqn. (3.8) has no counterpart in our previous work. Indeed, it is the implied formation of a horizontal salinity structure, consequent upon eqns. (2.19) and (2.20), that supports the baroclinic pressure gradient terms in eqn. (3.3). In turn, this leads to the formation of a two-layer flow structure characteristic of that observed in the Bosphorus. Accordingly, it is crucially important that the finite-difference analogue of eqn. (3.7) be correctly formulated and that this be compatible with eqns. (2.19) and (2.20). To achieve this end, appeal is made to a discretization of the horizontal advection term in eqn. (3.8) essentially based on one described by Roache (1972). This involves the application of a scheme of upstream differencing appropriate to a reversing flow and, at the same time, ensures global conservation. Consequently, we obtain a strict fulfilment of the necessary requirement that any change in the total salinity in the channel be balanced solely by the advective fluxes of salinity across $x = 0$ and $x = L$. (The diffusive flux of salinity across the end points of the channel is dropped from the formulation.)

The treatment of all terms in eqn. (3.8) other than the horizontal advection is analogous to our evaluation of the corresponding terms in eqn. (3.3) and is not detailed here. We simply describe the basic form of the solution process to be applied to

$$\frac{\partial \tilde{S}}{\partial t} + \frac{\partial}{\partial x}(\tilde{u}S) = \mathscr{R} \tag{4.6}$$

where $\mathscr{R}$ incorporates the effects of vertical advection, vertical diffusion and horizontal diffusion.

The finite-difference analogue of eqn. (4.6) has the form

$$\frac{\tilde{S}_{ij}^{p+1} - \tilde{S}_{ij}^p}{\Delta t} + \frac{1}{4\Delta x}\left[\left(\tilde{u}_{i+1j}^p - |\tilde{u}_{i+1j}^p|\right)S_{i+2j}^p + \left(\tilde{u}_{i+1j}^p + |\tilde{u}_{i+1j}^p| - \tilde{u}_{i-1j}^p + |\tilde{u}_{i-1j}^p|\right)S_{ij}^p + \left(-\tilde{u}_{i-1j}^p - |\tilde{u}_{i-1j}^p|\right)S_{i-2j}^p\right] = \mathscr{R}_{ij} \tag{4.7}$$

The terms in $\mathscr{R}_{ij}$ are evaluated partly implicitly and partly explicitly.

Analysis of eqn. (4.7) reveals that the horizontal advection scheme has a desirable upstream property that guarantees the positivity of computed values of $\tilde{S}$. When applied at $i = 1$ with $\tilde{u}^p_{0j} > 0$ (corresponding to inflow at $x = 0$), S^p_{-1j} must be prescribed and this is taken to be S_0 in which case eqn. (4.7) determines $\tilde{S}^{p+1}_{ij}$. However, if $\tilde{u}^p_{0j} < 0$ (corresponding to outflow at $x = 0$), $\tilde{S}^{p+1}_{ij}$ can be determined from eqn. (4.7) without reference to S^p_{-1j} which then no longer appears in the formulation of the horizontal advection. The only procedural problem is the determination of $\tilde{u}^p_{0j}$ which is not deducible from the updating of the velocity distribution because this is only carried out for $i = 2(2)m - 1$. Accordingly we have simply taken

$$\tilde{u}^p_{0j} = \tilde{u}^p_{2j} \tag{4.8}$$

which represents a simple extrapolation of the computed velocity from the Bosphorus into the Marmara Sea. Therefore, the computed dynamics of the Bosphorus model will imply whether a condition of inflow or outflow exists at $x = 0$ and eqn. (4.7) will then determine the corresponding local salinity conditions.

Similar comments may be made concerning the application of eqn. (4.7) for $i = m$. When $\tilde{u}^p_{m+1j} > 0$, there is outflow at $x = L$ and $\tilde{S}^{p+1}_{mj}$ is determined from eqn. (4.7) without reference to the salinity in the Black Sea. When $\tilde{u}^p_{m+1j} < 0$, there is inflow at $x = L$ and the determination of $\tilde{S}^{p+1}_{mj}$ involves a reference to S^p_{m+2j} which is taken to be S_L. Because the velocity is not updated at $i = m + 1$, we write

$$\tilde{u}^p_{m+1j} = \tilde{u}^p_{m-1j} \tag{4.9}$$

which represents an extrapolation of the computed velocity from the Bosphorus into the Black Sea.

The scheme given in eqn. (4.7) is discussed by Roache (1972, p. 73) under the heading of the second upwind scheme and is claimed to have desirable properties compared with the first upwind scheme. In spite of these, however, the scheme does imply the existence of numerical diffusion consequent upon its formal first-order accuracy. In our applications we have compensated for this, when $u > 0$, by extending the implied finite-difference approximation of the advective flux in eqn. (4.7) to formal second-order accuracy but have retained the upstream bias in the differencing. For $u < 0$, however, it was found necessary to retain the numerical diffusion implied by the first-order accurate scheme in order to avoid undesirable oscillations in the computed flow field. Given the uncertain contribution made by physical diffusion, the attendant advantages in using a slightly diffusive scheme appear to us to far outweigh the disadvantages. Our submission is that the fulfilment of the transportive condition and of global conservation is equally as important as the formal truncation error in the scheme. Indeed, our

method of implementation of the boundary conditions on the salinity at the ends of the channel is crucially dependent on the application of such a scheme.

Finally, it remains to parameterize the horizontal eddy transfer coefficient, N, introduced in section 3. On purely dimensional grounds (cf. Stacey and Zedel, 1986), we write

$$N = \alpha \Delta x E^{1/2} \tag{4.10}$$

Here, the grid-increment, Δx, is taken as a horizontal-mixing length scale and α is a further disposable parameter that must be given a numerical value in the experiments. Evidently, this is the weakest part of the parameterization because there is no obvious criterion available for the selection of a value for α. Our procedure will be to choose the smallest possible value for α consistent with obtaining a stable numerical solution.

Nevertheless, eqn. (4.10) does have a plausible physical content—namely that the horizontal mixing coefficient will attain its maximal values in localized regions of high turbulence energy density. Such regions are anticipated to occur in the neighbourhood of a developing internal hydraulic jump where we expect there to be a high level of turbulence energy production.

The entire formulation so far has been sufficiently general to allow for the numerical development of unsteady solutions for the velocity and salinity fields in the channel. However, in the experiments to be described subsequently, we are only interested in obtaining a steady-state response to a forcing derived from a prescription of a steady-state value of u_L. Our solution technique will therefore be to prescribe all dynamical dependent variables as being zero at $t = 0$. Arbitrarily, we have also chosen $S = S_0$ for $0 \leqslant x \leqslant L$ when $t = 0$. We then integrate the governing equations forward in time and, with steady-state forcing, continue until the initial transient response is both radiated out of the analysis region and is essentially dissipated by the action of friction. The remaining steady-state fields will then represent the response to the prescribed steady-state forcing.

5. NUMERICAL EXPERIMENTS

We have chosen the length of the channel, L to be 32.2 km whereas the actual length of the Bosphorus is about 31.0 km. This choice allows for the partial extension of the model channel into the Marmara Sea. The arrangement is depicted in Fig. 1 where the actual geometry of the Bosphorus is also delineated. To assist in the discussion of our results, we have selected five locations along the Bosphorus (labelled A–E) and have marked the corresponding approximate positions of these in the model channel.

The variation of the breadth and depth along the channel is difficult to prescribe uniquely. Indeed, in the first experiment to be described, we consider the flow through a channel having a uniform breadth and depth. It is only in the final experiment that an attempt is made to incorporate a geometry representative of that in the Bosphorus. In this case, inspection of the relevant British Admiralty chart suggests that the modelling of the numerous lateral inlets by appropriate choice of $b(x)$ will almost certainly misrepresent the geometry of the channel containing the principal component of the flow. Therefore, we decided to dispense with the frequent practice of estimating cross-sectional areas and mean depths and then inferring a corresponding value for $b(x)$. Instead, we choose values for $b(x)$ essentially based on the breadth of the navigation channel delineated on the British Admiralty chart no. 1198 of the Bosphorus. The minimum value of $b(x)$ is about 0.6 km and its maximum value is about 2.5 km. Values of $h(x)$ are chosen on the basis of an estimate of average depths across the chosen channel. They lie between 30 m at the sill near the Marmara Sea and a maximum of 80 m at the point of communication with the Black Sea. The profile of $h(x)$ along the channel is delineated in the figures depicting the computed results for the final experiment that incorporates a representation of the actual channel geometry.

The resolution in the finite-difference grid is fixed by taking $m = 89$ and $n = 21$. This implies that the distance between successive elevation (or current) points is about 731.8 m. The prescription of 21 computational levels in the vertical implies a vertical grid-spacing varying between 1.5 m above the sill and 4 m in the region of maximum depth.

With our scheme of discretization, the attainment of computational stability in the solution procedure is conditional only upon the time step, Δt, being limited by a quantity involving Δx and the barotropic gravity wave speed. In fact, our early experiments showed that computational stability is secured by taking $\Delta t = 15$ s. Consequently, we have retained this setting throughout our subsequent computations.

Preliminary experimentation was also used to ascertain suitable values for the turbulence parameters β and α appearing in eqns. (2.11) and (4.10). We found that a satisfactory vertical structure in the flow field is obtained by taking $\beta = 0.5\ \mathrm{m}^{-1}$. Therefore, within a bottom boundary layer for which $z + h < 2.0$ m, the difference between l and l_0 is never greater than 25%. For $z + h \gg 2.0$ m, however, the vertical mixing length scale is substantially reduced in comparison with l_0 and it is this feature of the parameterization that allows for the development of a two-layer type of flow structure.

In the experiments to be described here, we have taken $\alpha = 10.0$. Some preliminary calculations were performed using smaller values of α but the results were unsatisfactory and suggested that the horizontal mixing was

then insufficient to suppress the development of localized sharp horizontal gradients in the computed flow field.

The prescription of the bottom roughness in the channel is completed by taking $z_0 = 1$ cm. This implies that the effect on the flow of the roughness at the floor of the channel is equivalent to that of a rippled sand structure.

As already explained, the first experiment relates to the flow through a channel of uniform breadth and depth. Qualitatively, the solution for the flow structure is now independent of the value chosen for the breadth. However, it is most realistic to select values for the breadth and depth which yield a net volume transport representative of that estimated in the Bosphorus. Suitable values are found to be respectively 1.5 km and 70.0 m. Additionally, we choose a parameter setting in which

$$\left.\begin{aligned} u_L &= 0.125 \text{ m s}^{-1} \\ S_0 &= 38.5 \text{ ppt} \\ S_L &= 17.0 \text{ ppt} \end{aligned}\right\} \qquad (5.1)$$

This will be found to give rise to a net through-volume transport in the channel amounting to about 8573 m^3 s^{-1}.

Starting from a state of rest and a uniform salinity of 38.5 ppt in the channel, an effectively steady-state dynamical response is attained after about 7 days of integration. The computed salinity structure in the channel

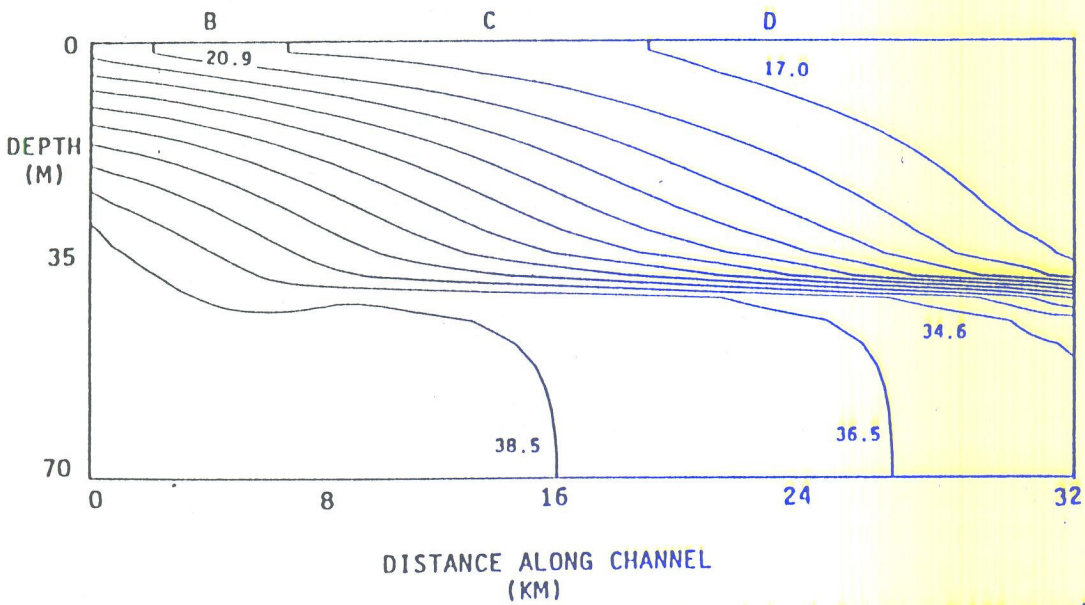

Fig. 2. Computed salinity in a channel of uniform breadth and depth for $u_L = 0.125$ m s^{-1}. Contour interval is 1.9 ppt.

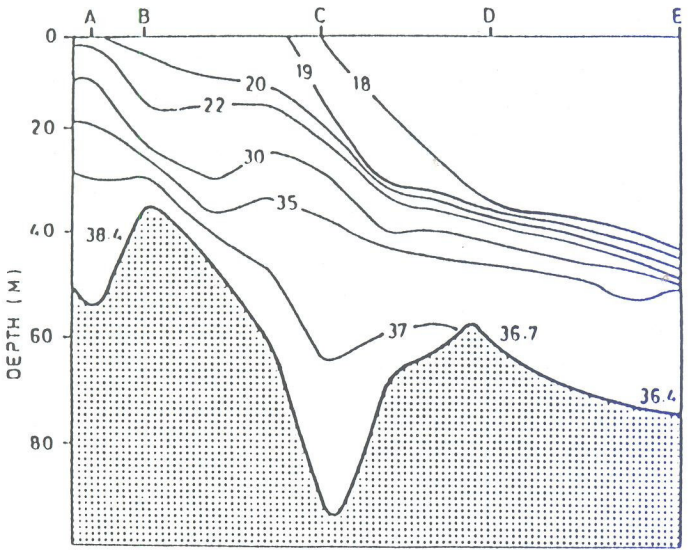

Fig. 3. Measured salinity in the Bosphorus in ppt during November 1985.

is depicted in Fig. 2. Although we have not yet incorporated the channel geometry into the experiment, it is informative to show in Fig. 3 a typical mid-channel salinity transect along the Bosphorus determined by Turkish oceanographers in November 1985 and described by Ozsoy et al. (1986). A comparison of the computed and observational results appears to show remarkably good agreement. Near the Black Sea end of the channel, the model reproduces the observed strong salinity gradient in the mid-depths. The 18 ppt salinity contour crops out at the surface of the channel in basically the correct position. The Marmara Sea end of the channel corresponds to a cropping out of the 21 ppt salinity contour. We note also that the 37 ppt salinity contour intersects the floor of the channel in approximately the correct longitudinal location and that there is a predicted existence of bottom water with salinity 35 ppt at the Black Sea end of the channel. Our submission, therefore, is that the gross features of the salinity structure in the Bosphorus are independent of its geometrical detail and may be reproduced by an appropriate choice of uniform rectangular cross-sectional area.

To illustrate the associated circulation pattern in the channel, it is convenient to introduce into eqn. (2.2) a streamfunction, ψ, such that

$$\left.\begin{aligned} b(x)u &= -\frac{\partial \psi}{\partial z} \\ b(x)w &= \frac{\partial \psi}{\partial x} \end{aligned}\right\} \tag{5.2}$$

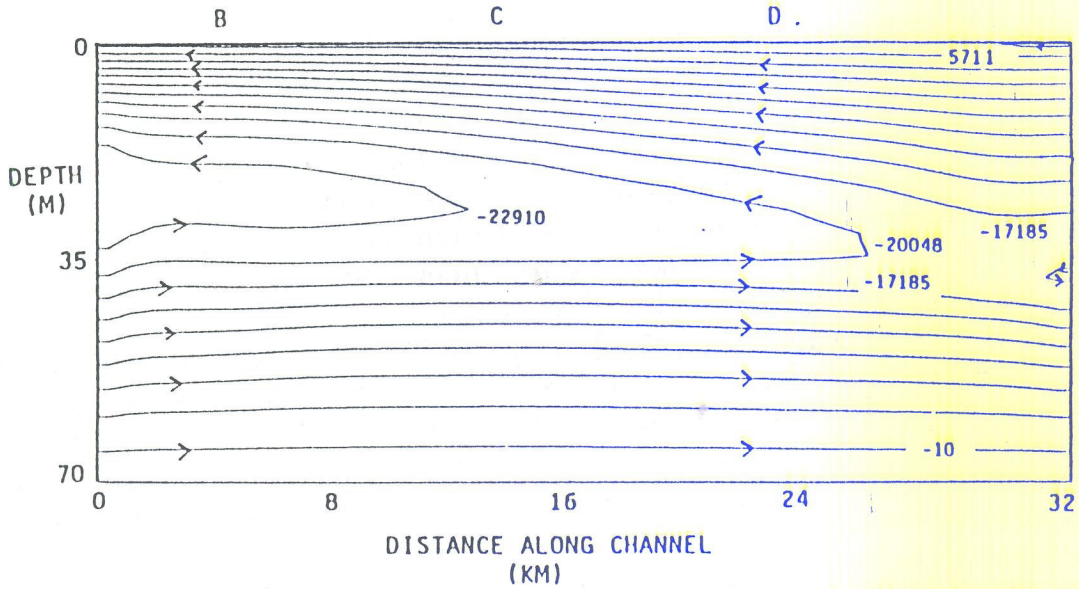

Fig. 4. Computed streamlines of the volume transport in a channel of uniform breadth and depth for $u_L = 0.125$ m s^{-1}. Contour interval is 2862 m^3 s^{-1}. Free surface streamline corresponds to 8573 m^3 s^{-1}.

the horizontal differentiation being at a fixed value of z. Accordingly, in terms of the σ-coordinate formulation,

$$\frac{\partial \psi}{\partial \sigma} = -bHu \tag{5.3}$$

and, on taking $\psi = 0$ at $\sigma = 0$,

$$\psi = -bH \int_0^{\sigma} u \, d\sigma \tag{5.4}$$

Therefore, by using the values of u at the discrete σ-levels, the integral in eqn. (5.4) may be evaluated numerically to yield the corresponding values of ψ. The streamlines of the volume transport in the channel are then delineated by plotting the contours along which ψ is a constant.

For the case of the uniform channel, the streamlines of the volume transport are shown in Fig. 4. The numbers on these refer to transport rates in m^3 s^{-1}, and show a surface flow directed towards the Marmara Sea of 25758 m^3 s^{-1}. Additionally, there is a uniform bottom flow directed towards the Black Sea of 17185 m^3 s^{-1} implying a net flow into the Marmara Sea of 8573 m^3 s^{-1}. It should be noted that there is an intermediate layer between the surface and bottom layers in which there is no net horizontal transport. This layer is characterized by the predicted existence of a recirculatory system in which a streamline entering the channel from the Marmara Sea continues almost to the Black Sea before turning back towards the Marmara

Sea. The region therefore constitutes an entrainment zone between the surface and bottom layers and all exchanges between these layers involve the mesoscale dynamics in this intermediate layer. It should be appreciated, however, that the structure of this zone is likely to be radically changed by the introduction of geometrical non-uniformity into the model.

It is necessary to discuss the implied salinity flux through the channel resulting from the use of eqn. (5.1). It is found that our solution implies a net salt flux into the Black Sea of the order of 1.2×10^5 kg s^{-1}. Because there is no steady-state sink of salt in the Black Sea, there might appear to be an inconsistency here with our steady-state solution. In a strict sense the net salt flux implied by the steady-state solution should be identically zero. It will be apparent, however, that our model is not characterized by the prescription of salt fluxes at the ends of the channel. The only disposable parameters are u_L, S_0 and S_L. Undoubtedly, the magnitude of u_L may be adjusted so as to obtain a steady-state solution in which there is no net salt flux through the channel and this procedure was applied in some of our early experiments. The resulting dynamical structure then corresponds to a physically realizable steady-state in which the net through transport of water is fixed and which, for prescribed values of S_0 and S_L, cannot vary in response to the observed seasonal variability in the Black Sea outflow. The attainment of such a condition, however, may only be achieved by extensive and time-consuming numerical computation and the implementation of an iterative routine in which the net salt flux is systematically reduced to zero. Given our limited computational resources, it soon became apparent to us that this approach is impracticable and the procedure was abandoned. Nevertheless, given the seasonal variability in the outflow of water from the Black Sea, it should be noted that, for limited periods of time, it is physically quite acceptable for there to be a net flux of salt either out of or into the Black Sea. For example, an increase in the value of S_L by 1 ppt would, with an assumed unchanged flow-rate as computed in the present experiment, reduce the implied flux of salt into the Black Sea by about 2×10^4 kg s^{-1}. Over an extended period of time the only requirement is that the net salt flux should average to zero thus implying a long term constant average salt content in the Black Sea.

The outcome of this discussion is that our solution may be viewed as being physically realizable during limited periods of the annual cycle. Without detailed information being available on the seasonal variations of S_0 and S_L which, when combined with the computed velocity u, determine the salt flux through the channel, it does not seem possible to apply the model in an inherently different way from that described here.

In Fig. 5, we show the associated computed velocity profiles at a sequence of positions along the channel. In these, the maximum velocity, which occurs

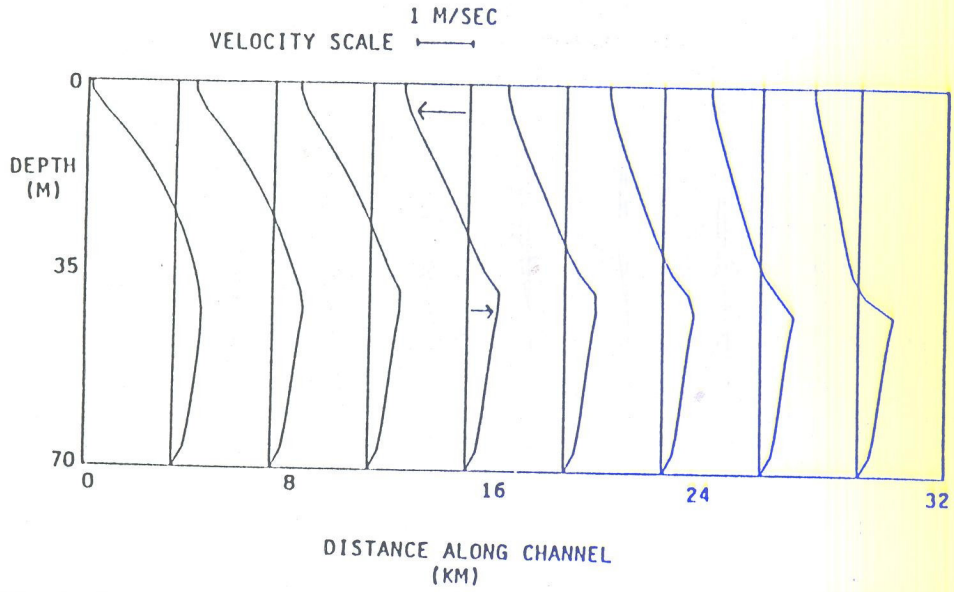

Fig. 5. Computed velocity profiles at a sequence of positions along a channel of uniform breadth and depth for $u_L = 0.125$ m s^{-1}.

at the surface near the Marmara Sea end of the channel, is approximately 1.5 m s^{-1}. We note that the level of velocity reversal becomes progressively deeper as the Black Sea end of the channel is approached and that this is accompanied by a weak progressive increase in the maximum current speed in the lower layer and a decrease in the upper layer. The corresponding difference in the surface elevation between the ends of the channel is 24 cm.

To complete the discussion of the uniform channel case, we have depicted in Fig. 6 profiles of the eddy viscosity at a sequence of positions along the channel. The maximum values are of the order of 0.14 m^2 s^{-1} and are encountered in the lower-layer flow that is directed towards the Black Sea. However, the important point to note is the marked reduction in the eddy viscosity to an almost laminar value in the mid-depths where the suppressive effect of the strong stable stratification on turbulence generation is at its greatest. This is an essential ingredient in the model and is necessarily required for the development of an effectively two-layer flow.

In the second experiment, we retain a constant depth of 70 m in the channel but incorporate the variation in breadth described earlier in this section. The parameter setting (5.1) remains the same. In Fig. 7, we depict the salinity contours corresponding to about 7 days of integration from an initial state rest. There is a marked difference between these contours and those shown in Fig. 2. Indeed, the comparison with the observed isolines in Fig. 3 appears to be inferior in quality. A predicted horizontal layer of strong vertical salinity stratification now extends along the entire length of

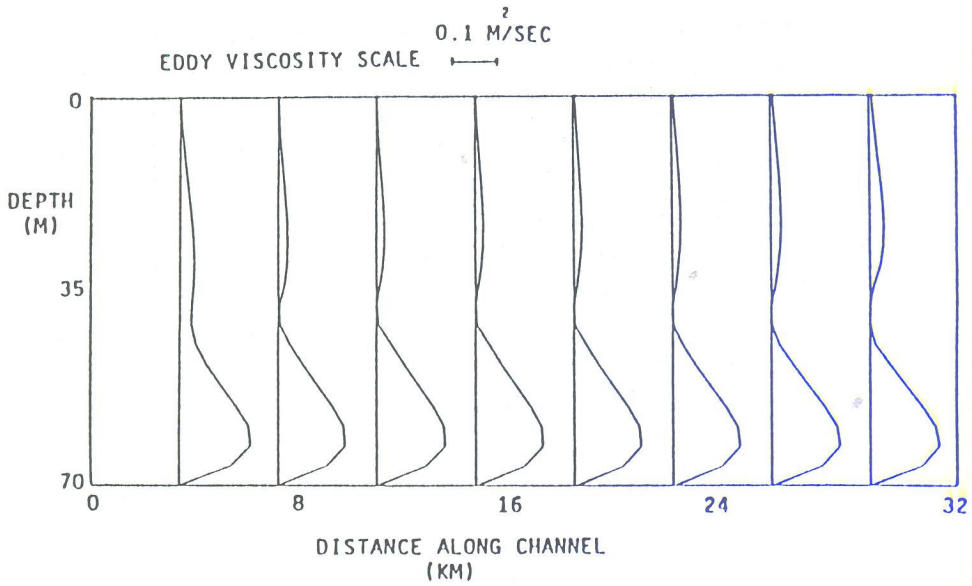

Fig. 6. Computed eddy viscosity profiles at a sequence of positions along a channel of uniform breadth and depth for $u_{l_s} = 0.125$ m s^{-1}.

the channel. Water having a salinity of about 17 ppt is found at the surface near the Marmara Sea end of the channel but this is considerably lower than the 22 ppt suggested by observational studies. A noteworthy feature of the computed salinity distribution is the occurrence of two regions of weak

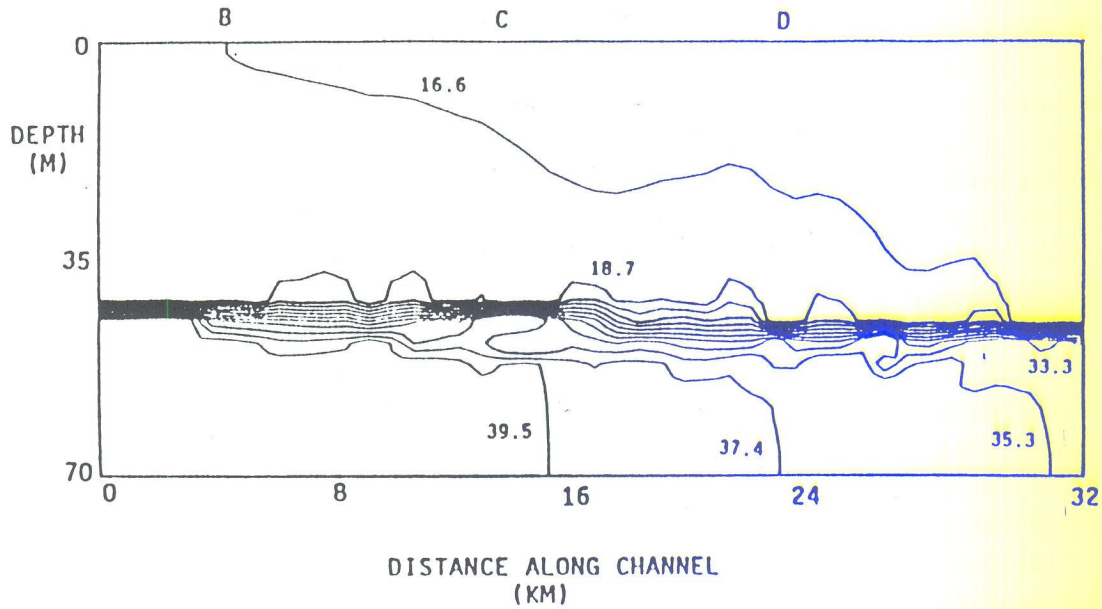

Fig. 7. As Fig. 2 except that the channel is of variable breadth. Contour interval is 2.1 ppt.

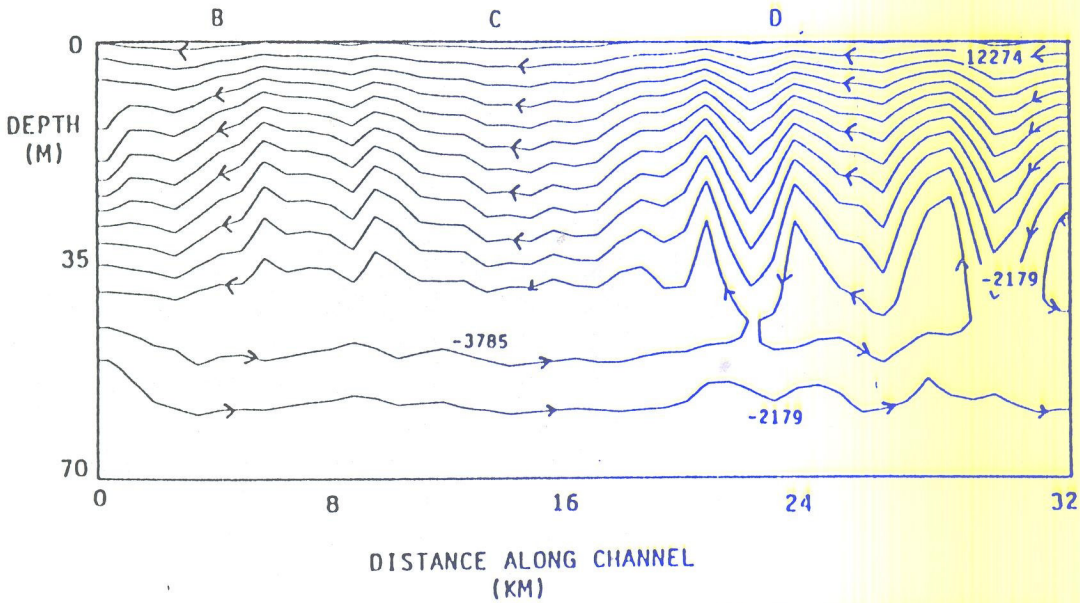

Fig. 8. As Fig. 4 except that the channel is of variable breadth. Contour interval is 1606 m^3 s^{-1}. Free surface streamline corresponds to 13880 m^3 s^{-1}.

instability beneath the layer of strong salinity stratification. Their position appears to correspond to the regions of channel contraction at C and D. Their occurrence prevents the attainment of a completely steady-state response because the associated unstable density stratification acts through the turbulence energy equation to generate additional turbulence energy and thus to enhance the local mixing. Accordingly, the local instabilities in the salinity field lead to the formation of ever-present transient features in the dynamical field.

In Fig. 8, we show the associated streamlines of the volume transport. Compared with those shown in Fig. 4, these no longer have a predominantly horizontal structure. There is now a pronounced waviness along the channel which correlates with the breadth variations delineated in Fig. 1. Moreover, corresponding to the breadth variations near the Black Sea end of the channel, we note the prediction of a closed circulation cell in the entrainment zone between the upper and lower layers. The use of $u_L = 0.125$ m s^{-1} leads to a relatively high net through transport of about 13880 m^3 s^{-1} and a lower-layer transport of 2179 m^3 s^{-1}, therefore implying an upper layer transport of 16059 m^3 s^{-1}. Compared with observational estimates of typical volume transports in the layers, the computed transports are relatively inconsistent as they should be in a ratio of about 3 to 1. Accordingly, it is suggested that the incorporation of bottom topography into the model is required in order to counteract some of the dynamical effects associated solely with variations in the breadth.

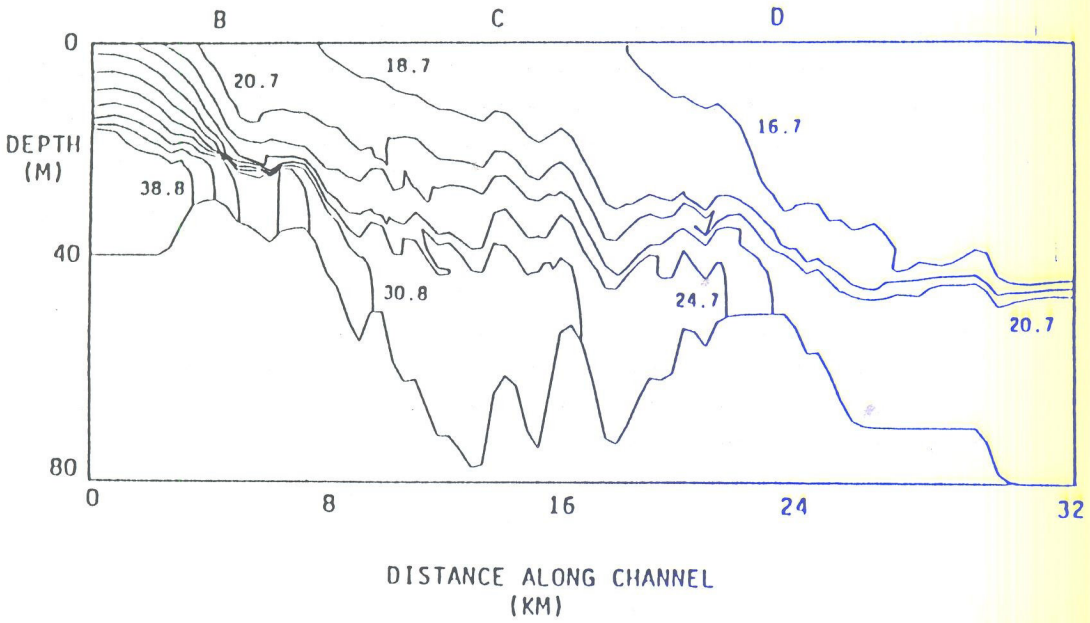

Fig. 9. As Fig. 2 except that the channel is of variable breadth and depth and $u_L = 0.1$ m s^{-1}. Contour interval is 2.0 ppt.

Considering the implied salt balance in the system, we find that there is now a net salt flux out of the Black Sea amounting to about 1.3×10^5 kg s^{-1}. The only change made here is the incorporation of breadth variations into the channel topography and this results in a reversal in the direction of the net salt flux. The implied sensitivity of the model response to a change in the geometry of the channel is indicative of the difficulties that may be expected in an attempt to adjust the value of u_L so as to obtain a condition of zero net salt flux in a steady-state solution. Accordingly, we prefer simply to use a parameter setting which yields a net volume transport of water through the channel that is consistent with observationally estimated average values and to regard the implied net salt flux as being a seasonally variable quantity that is correlated with the net flux of water leaving the Black Sea.

In the final experiment, we incorporate the full breadth and depth variations along the channel described earlier in this section. We again use the parameter setting (5.1) with the exception that now $u_L = 0.1$ m s^{-1}. Salinity contours corresponding to an effectively steady-state response are shown in Fig. 9. We note the predicted existence of surface water with a salinity in excess of 22 ppt at the Marmara Sea end of the channel. In comparison with the salinity contours shown in Fig. 2, there is now a significantly sharper horizontal gradient in the salinity field in this region. This is more in accord with the observed salinity structure shown in Fig. 3

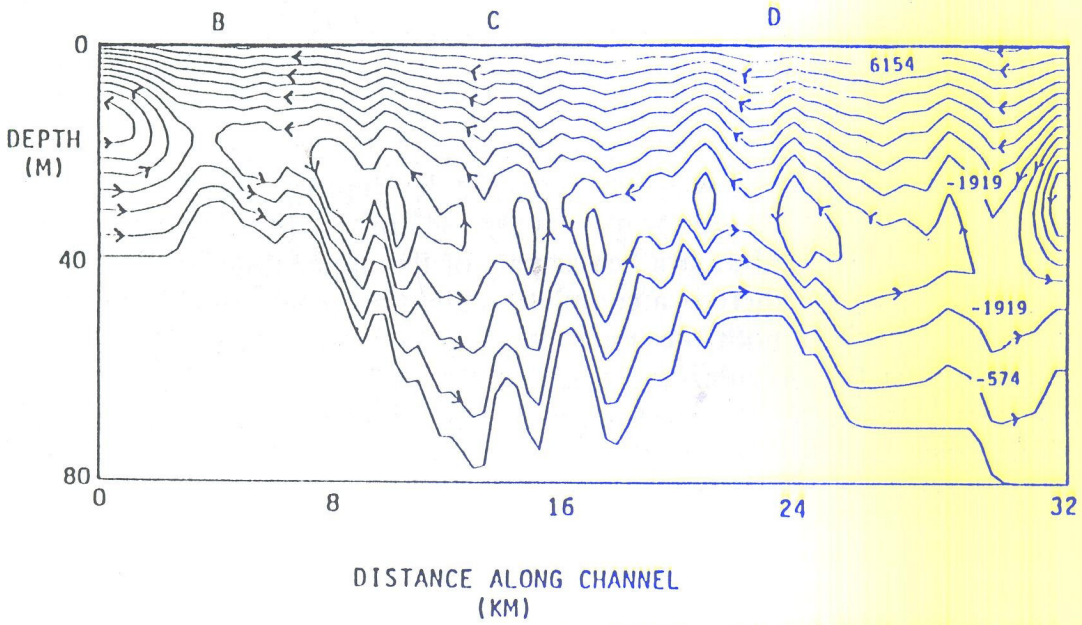

Fig. 10. As Fig. 4 except that the channel is of variable breadth and depth and $u_L = 0.1$ m s^{-1}. Contour interval is 1345 m^3 s^{-1}. Free surface streamline corresponds to 7499 m^3 s^{-1}.

and is therefore associated with the sill that now occupies this region. Nevertheless, in comparison with the observed salinity structure, the model seems unable to admit the penetration of high-salinity bottom water beyond the sill and into the central regions of the channel. The combined presence of the three regions of relatively shallow water in the channel acts to prevent water with a salinity in excess of 22 ppt from penetrating into the Black Sea. This is not in accord with any observational study and, in the light of our previous experiments, is attributed to our specification of the bottom topography. We are therefore led to suggest that the actual flow through the Bosphorus is inextricably three-dimensional in structure. The sill at the Marmara Sea end of the channel does not (as in our model) extend completely across the channel but is an isolated feature in the mid-channel. In actuality, the lower-layer flow is therefore able to pass around as well as over the sill, In our model, however, the entire flow must pass over the sill and, as will be seen by examining the corresponding computed streamlines, this is dynamically impossible to achieve with a lower-layer transport comparable with that known to exist in the Bosphorus.

The corresponding streamlines of the computed volume transport are delineated in Fig. 10. From these, we note that a setting in which $u_L = 0.1$ m s^{-1} leads to a net through transport of 7499 m^3 s^{-1}. The lower-layer transport amounts to about 1919 m^3 s^{-1} and the upper-layer transport is 9418 m^3 s^{-1}. Relative to the upper-layer transport, that in the lower layer appears to be significantly underestimated. This model result is a conse-

quence of the substantial recirculatory system that develops in the entrainment zone and which is so apparent in Fig. 10. As is readily seen, a lower-layer flow amounting to more than 3264 $m^3\ s^{-1}$ enters the channel from the Marmara Sea. This is approximately 34% of the upper-layer flow. However, the presence of the sill leads to the development of local upwelling and a mesoscale recirculation which causes 1345 $m^3\ s^{-1}$ of the incoming flow to be returned to the Marmara Sea as part of the upper flow. Thus, at some height above the sill, there is a complete stagnation region in the Reynolds-averaged flow where both the horizontal and vertical velocities are vanishingly small. At this singular point, the mechanical energy is in the form of pure turbulence. Clearly, such a region could not exist in a system lacking internal friction and its prediction here is evidently related to the form of our scheme of turbulence parameterization.

The corresponding net salt flux is found to be about 7.8×10^4 kg s^{-1} out of the Black Sea and the direction of the net salt flux is again reversed in comparison with the first experiment. The steady-state solution implies strictly that the salt content of the Black Sea will decrease. However, as we have suggested earlier, the solution is properly viewed as part of a realizable cycle in which seasonal variations may be expected to bring about an annually averaged zero net salt flux through the channel.

We also note from Fig. 10 the predicted existence of a series of intermediate-scale dynamical features within the recirculation zone that are equivalent to closed circulation cells with horizontal axes. The entire intermediate-layer regime will therefore play a prominent role in the exchange of water between the surface and bottom layers. In particular, we can offer an explanation for the increase in the salinity of surface water on the Marmara Sea side of the sill. Saline bottom water from the Marmara Sea is forced to recirculate and to appear as near-surface water which returns to the Marmara Sea. Naturally, the salinity values of this surface-water are modified by the action of the vertical mixing process but it does explain why, in Fig. 9, a surface salinity of 25 ppt is found between the sill and the Marmara Sea. It is tempting to identify the dynamics in this region with those that occur in a stationary hydraulic jump but it is not clear how to give quantitative support for this conjecture in a multi-layered system.

Likewise, near-surface water entering the Bosphorus from the Black Sea is predicted to recirculate and to appear as near-bottom water which ultimately exits from the Bosphorus and returns into the Black Sea. Thus, there is an entry of low-salinity water into the lower layer and a redistribution of this by vertical mixing. This explains the almost uniform salinity distribution produced in the model at its point of entry into the Black Sea. Independent support for the existence of a recirculation pattern in the Bosphorus having the gross features described here is given by Tolmazin (1985).

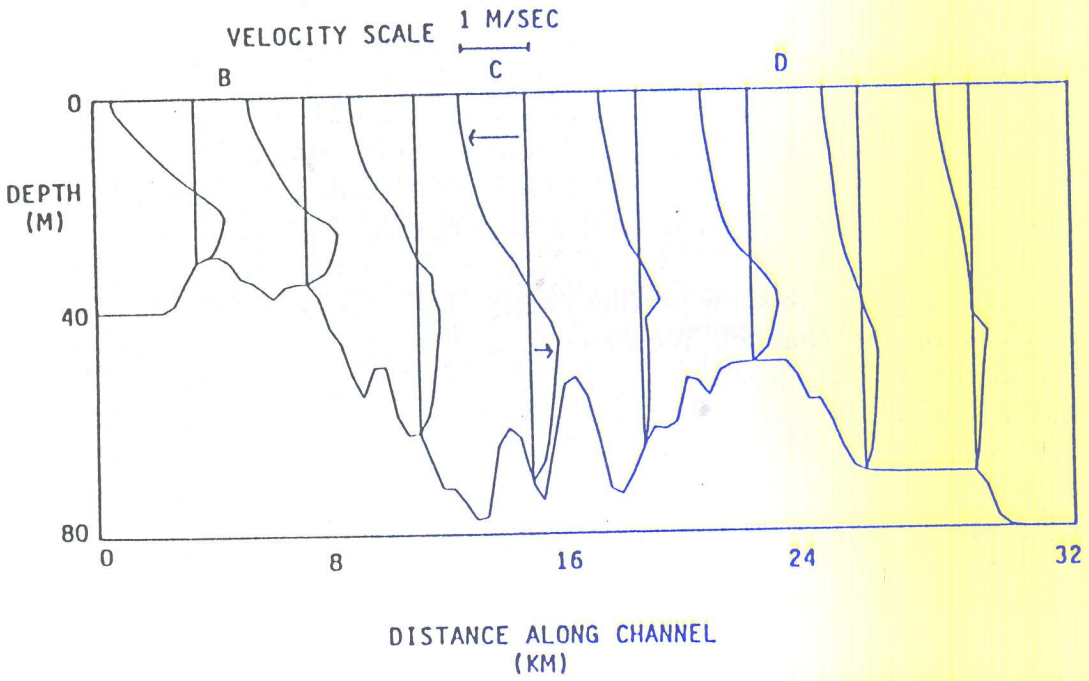

Fig. 11. As Fig. 5 except that the channel is of variable breadth and depth and $u_L = 0.1$ m s^{-1}.

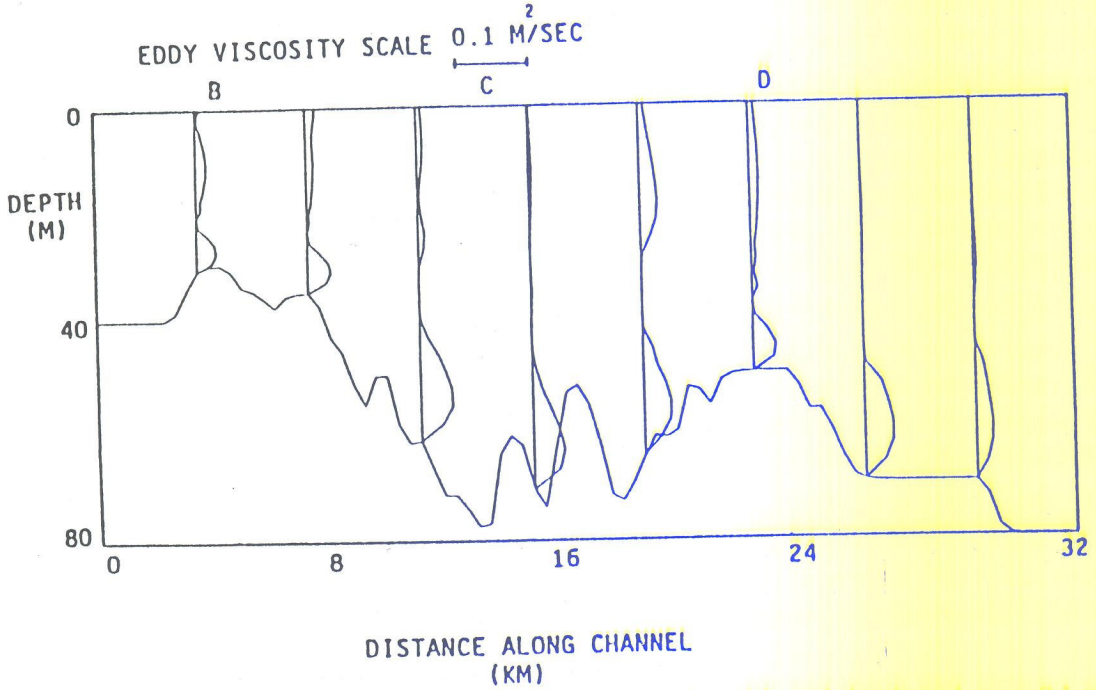

Fig. 12. As Fig. 6 except that the channel is of variable breadth and depth and $u_L = 0.1$ m s^{-1}.

To complete the discussion of the final experiment, we show in Fig. 11 velocity profiles at a sequence of positions along the channel. The maximum current speed of about 1.17 m s^{-1} occurs at the surface above the sill and the thickness of the lower-layer flow is a minimum at this position. We also note the marked acceleration in the surface flow as the sill is approached thus suggesting that there will be a trend towards supercritical conditions at this location.

Finally, in Fig. 12, we show profiles of the eddy viscosity at a sequence of positions along the channel. We again note a reduction in the turbulent mixing in the mid-depths that is required for the existence of a basically two-layer flow. There is also an indication of an increase in the mixing in the surface layer above the sill region, which is interpreted in terms of an enhanced turbulence energy production associated with an approach to the supercritical conditions found in a stationary internal hydraulic jump. Maximum values of the eddy viscosity encountered in the lower layer are of order 0.1 m^2 s^{-1} and occur in the vicinity of the sill.

6. CONCLUSIONS

Three experiments have been performed with a two-dimensional model to investigate the flow of water through the Bosphorus. In the first of these, it is shown that the gross features of the observed flow may be reproduced by selecting a model channel having a uniform rectangular cross-sectional area. The resulting flow structure consists basically of a two-layer system in which there is a through penetration in the lower layer of high-salinity water into the Black Sea.

In the second experiment, a longitudinal breadth variation is introduced into the model which remains two-dimensional in character. The two-layer flow structure is preserved for a net through transport of the order of that existing in the Bosphorus but there is evidence of the formation of an intermediate layer containing circulation cells that appear to be associated with variations in the breadth. A through transport of high-salinity water still occurs in the bottom layer but the relative values of the volume transports in the layers appear to be incorrect.

In the final experiment, variations in both the breadth and the depth are introduced into the two-dimensional model. These include a representation of the sill that exists at the Marmara Sea end of the channel. However, although the model produces a realistic salinity structure in the vicinity of the sill, it fails to admit the penetration of water with sufficiently high salinity into the Black Sea. This is attributed to a complex system of recirculation that forms in the intermediate layer and the fact (in two

dimensions) that all water must pass over the sill and that none may flow around it.

This leads us to suggest that the flow of water through the Bosphorus is inextricably three-dimensional in character and may only be satisfactorily simulated in a three-dimensional model, as opposed to the two-dimensional model utilized in this paper. The development of a three-dimensional model represents a major increase in complexity and computational requirements as compared with the model described in this paper. It would, however, admit the modelling of the numerous lateral inlets in the Bosphorus and might be expected to lead to the simulation of the observed surface eddies that result in local reversals in the direction of the surface current.

ACKNOWLEDGEMENT

The collaborative work reported here was made possible by the award of a NATO travel grant, RG. 85/0628.

REFERENCES

Assaf, G. and Hecht, H., 1974. Sea straits: a dynamial model. Deep-Sea Res., 21: 947–958.

Defant, A., 1961. Physical Oceanography, Vol. 1. Pergamon, Oxford, 729 pp.

Johns, B., 1978. The modeling of tidal flow in a channel using a turbulence energy closure scheme. J. Phys. Oceanogr., 8: 1042–1049.

Johns, B., 1983. Turbulence modelling beneath waves over beaches. In: B. Johns (Editor), Physical Oceanography of Coastal and Shelf Seas, Chap. 3, Elsevier Amsterdam, Oxford, New York, Tokyo, 470 pp.

Johns, B., Dube, S.K., Mohanty, U.C. and Sinha, P.C., 1981. Numerical simulation of the surge generated by the 1977 Andhra cyclone. Q. J. R. Meteorol. Soc., 107: 919–934.

Johns, B., Sinha, P.C., Mohanty, U.C., and Rao, A.D., 1983. Simulation of storm surges using a three-dimensional numerical model: an application to the 1977 Andhra cyclone. Q. J. R. Meteorol. Soc., 109: 211–224.

Kundu, P.K., 1984. Numerical calculations of coastal flow with turbulent dynamics. Deep-Sea Res., 31: 39–60.

Ozsoy, E., Oguz, T., Latif, M.A. and Ünlüata, Ü., 1986. Dynamics of the Turkish Straits. Report, Institute of Marine Sciences, Middle East Technical University, Turkey, 108 pp. (unpublished).

Roache, P.J., 1972. Computer Fluid Dynamics. Hermoza, Albuquerque, NM, 434 pp.

Stacey, M.W. and Zedel, L.J., 1986. The time-dependent hydraulic flow and dissipation over the sill of Observatory Inlet. J. Phys. Oceanogr., 16: 1062–1076.

Sumer, B.M. and Bakioglu, M., 1981. Sea-strait flow with reference to the Bosphorous. Report, Faculty of Civil Engineering, Technical University of Istanbul, 25 pp. (unpublished).

Tolmazin, D., 1981. Two dimensional circulation in straits. Ocean-81, Proceedings of IEEE Conference, September 1981, Boston, MA, pp. 820–823.

Tolmazin, D., 1985. Changing coastal oceanography of the Black Sea. II. Mediterranean effluent. Prog. Oceanogr., 15: 277–316.

Ünlüata, Ü. and Oguz., T., 1983. A review of the dynamical aspects of the Bosphorous. Report, Institute of Marine Sciences, Middle East Technical University, Turkey, 42 pp. (unpublished).

Wang, D.P., 1987. The strait outflow. J. Geophys. Res., 92: 10807–10825.